ISSN 1063-7834, Physics of the Solid State, 2017, Vol. 59, No. 7, pp. 1291–1297. © Pleiades Publishing, Ltd., 2017.
Original Russian Text © S.V. Semenov, D.A. Balaev, M.A. Pochekutov, D.A. Velikanov, 2017, published in Fizika Tverdogo Tela, 2017, Vol. 59, No. 7, pp. 1267–1273.

SUPERCONDUCTIVITY

Anisotropy of the Magnetoresistive Properties of Granular High-Temperature Superconductors Resulting from Magnetic Flux Compression in the Intergrain Medium

S. V. Semenov[a, b]*, D. A. Balaev[a, b], M. A. Pochekutov[a, b], and D. A. Velikanov[a]

[a] *Kirensky Institute of Physics, Federal Research Center KSC SB RAS, Krasnoyarsk, 660036 Russia*
[b] *Siberian Federal University, Krasnoyarsk, 660036 Russia*
**e-mail: svsemenov@iph.krasn.ru*

Received November 16, 2016

Abstract—To elucidate the origin of the well-known anisotropy of the magnetoresistive properties of granular high-temperature superconductors (HTSs), which is related to the mutual orientation of magnetic field **H** and transport current **j**, we investigate the hysteretic dependences of magnetoresistance $R(H)$ of the yttrium HTS sample at the perpendicular ($\mathbf{H} \perp \mathbf{j}$) and parallel ($\mathbf{H} \parallel \mathbf{j}$) configurations. The hysteretic $R(H)$ dependences are analyzed using the concept of the effective field in the intergrain boundaries through which superconducting current carriers tunnel. The effective degree of magnetic flux compression in the intergrain medium at the perpendicular configuration was found to be twice as much as at the parallel one. This approach explains well the anisotropy of the magnetoresistive properties of granular HTSs, which was previously reported by many authors, and the temperature dependences of the resistance in the resistive transition region.

DOI: 10.1134/S1063783417070241

1. INTRODUCTION

As is known, granular high-temperature superconductors (HTSs) demonstrate the anisotropy of magnetoresistance $R(H)$ and resistive transition $R(T)$ at different mutual orientations of magnetic field **H** and transport current **j** (hereinafter, vector **j** corresponds to the macroscopic direction of the current flowing in a sample) [1–13]. On one hand, this is no surprise, since in the classical Bardeen–Stephen consideration the magnetoresistance of the second-order semiconductors, which depends on the angle $\theta = \angle\mathbf{H}, \mathbf{j}$, is proportional to $\sin^2\theta$ [14]. The rate of energy dissipation on the vortex length depends on the product of the Lorentz force and vortex velocity [14, 15]; since the vortex motion is induced by the Lorentz force, the vortex velocity is proportional to $\sin\theta$ and, therefore, we have $R \sim \sin^2\theta$.

On the other hand, the observed dependence of the magnetoresistance on angle θ for granular HTSs is caused by the processes occurring in the randomly oriented intergrain boundaries; in this case, HTS crystallites (grains) are also randomly oriented. The intergrain boundaries are regions with suppressed superconducting properties, which behave like Josephson junctions through which superconducting current carriers tunnel. The nature of the magnetoresistance anisotropy in such a random system requires special consideration.

Certain progress in understanding this anisotropy was made in [7], where the magnetic fields induced by screening currents on the surface of superconducting grains were assumed to significantly contribute to the magnetic induction in the intergrain medium. Although the authors of [7] obtained good agreement between the experimental and model dependences of the value $R(\mathbf{H} \perp \mathbf{j})/R(\mathbf{H} \parallel \mathbf{j})$ on the applied field, they did not directly determine the effective field in the intergrain medium.

The technique for determining the effective field in the intergrain medium and degree of magnetic flux compression in the intergrain spacings directly from the experimental data on magnetization and magnetoresistance was proposed in [16–18]. The aim of this work was to determine these quantities at $\mathbf{H} \parallel \mathbf{j}$ and $\mathbf{H} \perp \mathbf{j}$ in order to unambiguously establish the origin of the observed anisotropy of the magnetoresistive properties of granular HTSs.

2. MODEL

Let us consider a schematic of the distribution of local fields induced by the magnetic moments of superconducting grains in the intergrain medium. Figure 1a shows the distribution of lines of magnetic

induction $\mathbf{B}_{ind}$ for two grains separated by a sufficiently large distance and located in the increasing applied field $H = H_{\uparrow}$. Here, $\mathbf{M}_G$ is the magnetic moment of an individual grain, which is directed antiparallel to the applied field at $H = H_{\uparrow}$, and the $\mathbf{B}_{ind}$ distribution is only related to $\mathbf{M}_G$. Each point beyond the grain is affected by the local field $\mathbf{B}_{local}(\mathbf{r})$, which is superposition of $\mathbf{B}_{ind}(\mathbf{r})$ and applied field $\mathbf{H}$:

$$\mathbf{B}_{local}(\mathbf{r}) = \mathbf{H} + \mathbf{B}_{ind}(\mathbf{r}).$$

Since the $\mathbf{B}_{ind}(\mathbf{r})$ value is related to $\mathbf{M}_G$, we can write

$$\mathbf{B}_{local}(\mathbf{r}) = 4\pi\mathbf{M}_G\mathbf{K}(\mathbf{r}) + \mathbf{H}, \quad (1)$$

where $\mathbf{K}(\mathbf{r})$ depends on the geometrical parameters of the grain and distributions of the screening currents and flux trapped in it.

If we bring two grains close to each other (Fig. 1b), as in polycrystalline materials, the lines of magnetic induction $\mathbf{B}_{ind}$ between grains A and B will obviously be significantly crowded. Then, in the region of our interest (between grains A and B in Fig. 1b), we can introduce effective field $\mathbf{B}_{eff}$, which, after averaging over local fields (1), will be related to the sample magnetic moment $\mathbf{M}$ as

$$\mathbf{B}_{eff} = 4\pi\mathbf{M}\alpha + \mathbf{H}. \quad (2)$$

Parameter α arises upon averaging $\mathbf{K}(\mathbf{r})$ in Eq. (1) and characterizes the degree of crowding of the magnetic induction lines related to the grain magnetic moments.

Equation (2) explains the origin of the magnetoresistance hysteresis $R(H)$ in granular HTSs: $R \propto |B_{eff}|$ (ignoring the details of the functional dependence $R(\boldsymbol{B}_{eff})$) and the magnetic moment $M(H)$ of the sample is a hysteretic function of the applied field (Fig. 2). When the applied field increases, we have $M(H_{\uparrow}) < 0$. When the field decreases ($H_{\downarrow} = H_{\uparrow}$), we have $M(H_{\downarrow}) > M(H_{\uparrow})$, or the $M(H_{\uparrow})$ value is positive in a certain field range (Fig. 2). If the magnetic moment M is negative ($M < 0$ at $H = H_{\uparrow} > 0$), then the field induced in the spacing between grains A and B is codirected with the applied field (Fig. 1b). At $M > 0$ ($H = H_{\downarrow} > 0$), the $\mathbf{B}_{ind}$ direction between grains A and B is opposite to the $\mathbf{H}$ direction (the arrows indicating the direction of magnetic induction lines in Fig. 1b change their direction for the opposite one). Hence, taking into account the sign of the $M(H)$ dependence, we obtain the effective field in the intergrain medium determined by Eq. (2):

$$B_{eff}(H_{\uparrow}) = -4\pi M(H_{\uparrow})\alpha + H_{\uparrow}, \quad (3)$$

$$B_{eff}(H_{\downarrow}) = -4\pi M(H_{\downarrow})\alpha + H_{\downarrow}. \quad (4)$$

Equations (3) and (4) allow us to estimate the degree of magnetic flux compression, i.e., coefficient α, which, as a rule, is much higher (by an order of magnitude) than unity [16–19]. The α value is determined using the obvious condition: if the experimental hysteretic dependence meets the condition

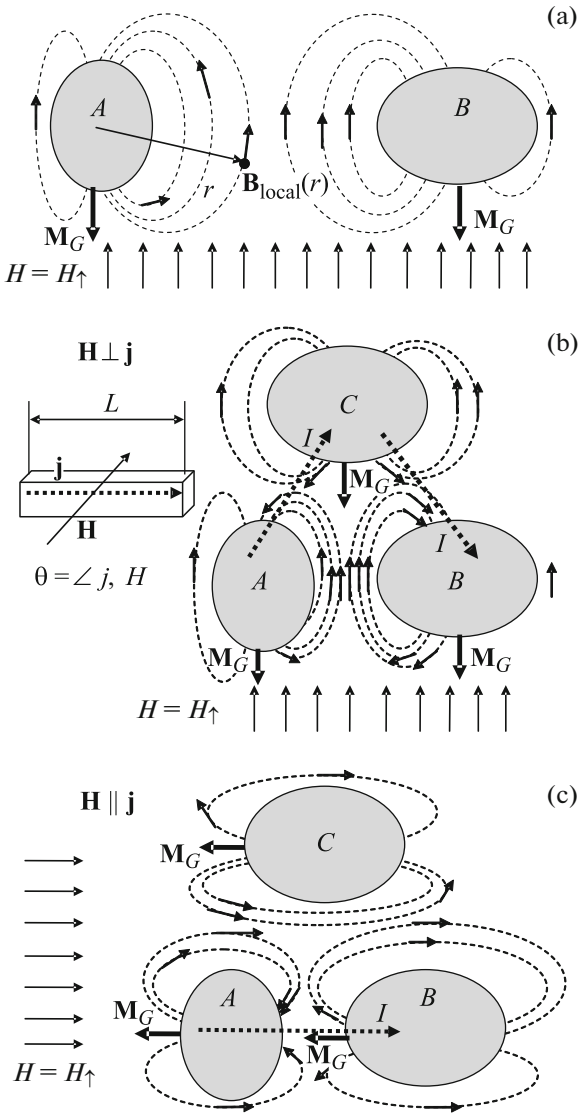

Fig. 1. Schematic of magnetic induction lines in the intergrain medium related to the magnetic moments of superconducting grains. (a) Grains are sufficiently far from each other and (b, c) magnetic induction lines are crowded at the sufficiently small intergrain distance. Schematic trajectories of microscopic currents I for (b) the perpendicular and (c) parallel configurations of $\mathbf{H}$ and $\mathbf{j}$. In all the cases, the applied field increases: $H = H_{\uparrow}$. (b, on the left) Scheme of the experiment.

$R(H_{\uparrow}) = R(H_{\downarrow})$, then $B_{eff}(H_{\uparrow}) = B_{eff}(H_{\downarrow})$. Thus, we obtain from (3) and (4)

$$\Delta H = H_{\downarrow} - H_{\uparrow} = \alpha 4\pi\{M(H_{\downarrow}) - M(H_{\uparrow})\}. \quad (5)$$

Using Eq. (5), we can determine the α value from the experimental hysteretic $R(H)$ and $M(H)$ dependences obtained on the same sample. The approximation of the weak magnetic field dependence of α ($\alpha \neq f(H)$) was found to be not bad, although in the field range corresponding to $M \approx 0$ (in this case, the contribution

of the trapped magnetic flux is similar to the diamagnetic contribution) the effect of magnetic moments of grains remains significant.

Let us now pass to the problem of flowing of microscopic currents **I** through the intergrain boundaries at $\mathbf{H} \parallel \mathbf{j}$ and $\mathbf{H} \perp \mathbf{j}$. At the perpendicular orientation, the current flow from grain *A* to grain *B* (Fig. 1b) will obviously be unfavorable, since at $\mathbf{I} \perp \mathbf{B}_{\text{eff}}$ the magnetoresistance will be maximum ($R \propto \sin^2\theta$, $\theta = \angle\mathbf{H}, \mathbf{j}$). Obviously, the path through the neighboring grain (*C*), at which the mutual orientation of **I** and B_{eff} is almost parallel (the path $A \rightarrow C \rightarrow B$ schematically shown in Fig. 1b), will be more favorable for the microscopic transport current. At $\mathbf{H} \parallel \mathbf{j}$, the optimal flow path is still $A \rightarrow B$ (Fig. 1c). Certainly, in this case, there are also many intergrain boundaries in which the parallel orientation of **H** and **j** is broken. This difference from the ideal parallel orientation manifests itself in the fact that even at $\mathbf{H} \parallel \mathbf{j}$ the coefficient α appears to be about 10. In [16–19], the measurements were performed for this very orientation. It would be reasonable to suggest that the α value for the same sample will by larger at $\mathbf{H} \parallel \mathbf{j}$ than at $\mathbf{H} \perp \mathbf{j}$. The experiments will finally confirm that it is the magnetic flux crowding (significant α value) that determines the observed magnetoresistance anisotropy (magnetic field–transport current) of granular HTSs.

3. EXPERIMENTAL

The $Y_{0.98}Pr_{0.02}Ba_2Cu_3O_7$ HTS was prepared by standard solid-state synthesis. The X-ray diffraction study revealed only 1-2-3 reflections. The $R(T)$ dependence of the sample above T_C (90.5 K) is of the metal type characteristic of such systems.

The transport measurements were performed on the samples with a typical size of ~(1 × 1 × 7) mm. The temperature dependences of magnetoresistance ($R(H) = U(H)/j$, where *U* is the potential drop and *j* is the transport current), and resistance ($R(T)$) were measured by a standard four-probe method. The transport current flew parallel to the long sample side. During the measurements of the $R(H)$ dependences (the data are given for $j = 30$ mA), the sample was immersed in liquid nitrogen. The external field was specified by an FL-1 electromagnet, which allowed measuring the transport characteristics for both the parallel ($\mathbf{H} \parallel \mathbf{j}$) and perpendicular ($\mathbf{H} \perp \mathbf{j}$) orientations. After zero-field cooling (ZFC), the external field was changed for the maximum applied field $H_{\text{app}} = \pm 500$ or ± 1000 Oe. Then, the data on the forward and reverse branches of the hysteretic dependences, except for the initial path from $H = 0$ to $H_{\text{app}} = +500$ Oe, were analyzed. The $R(T)$ dependences were measured under ZFC and field cooling (FC) conditions with the subsequent switching-off the field at the two orientations ($\mathbf{H} \parallel \mathbf{j}$ and $\mathbf{H} \perp \mathbf{j}$).

The magnetic measurements were performed on a vibrating sample magnetometer [20]. For this purpose, samples with the geometrical parameters similar to those used in the transport measurements (~(0.5 × 0.5 × 3.5) mm) were prepared. Therefore, the demagnetizing factor of the sample shape in the magnetic and transport measurements should be the same. The Puzei electromagnet-based setup [20] allows measurements at both $\mathbf{H} \parallel \mathbf{L}$ and at $\mathbf{H} \perp \mathbf{L}$, where **L** is the vector directed parallel to the long sample side. The applied field variation rate in the transport and magnetic measurements was the same (~2 Oe/s). The $M(H)$ and $M(T)$ dependences were measured under the same external conditions as the $R(T)$ dependences.

4. RESULTS AND DISCUSSION

4.1. Anisotropy of the Magnetoresistance R(H)

To correctly compare the $M(H)$ and $R(H)$ dependences, the magnetic measurements were performed at two mutual orientations of **L** (the long sample side) and applied field **H**. The $M_\perp(H)$ ($\mathbf{H} \perp \mathbf{L}$) and $M_\parallel(H)$ ($\mathbf{H} \parallel \mathbf{L}$) dependences for the investigated sample are shown in Fig. 2. It can be seen that the difference between the cases $\mathbf{H} \parallel \mathbf{L}$ and $\mathbf{H} \perp \mathbf{L}$ is minor (there is a small discrepancy between the $M_\perp(H)$ and $M_\parallel(H)$ dependences in the field range of 500–1000 Oe); the demagnetizing factor of the sample shape does not play a decisive role in the magnetic measurements of granular HTSs. The $M(H)$ hysteresis loop is typical of granular HTSs synthesized using a standard technique [21].

Figure 3 shows hysteretic $R(H)$ dependences for the parallel ($R_\parallel(H)$) and perpendicular ($R_\perp(H)$) mutual orientations of **H** and **j**. One can clearly see the afore-

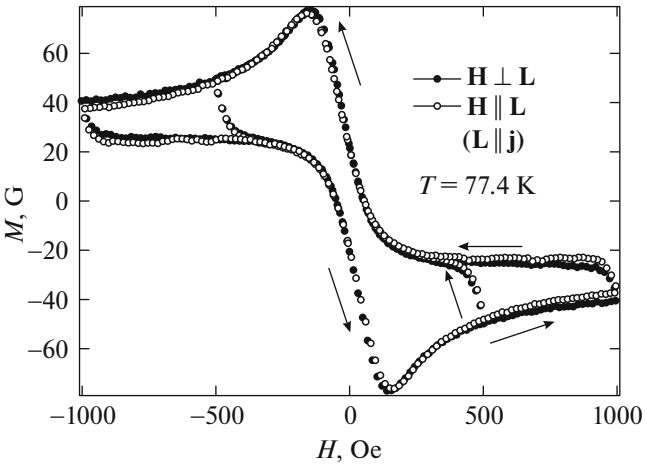

Fig. 2. $M(H)$ magnetic hysteresis loops for the investigated sample in maximum applied fields of $H_{\text{app}} = 500$ and 1000 Oe for the indicated configurations (scheme of the experiment is shown in Fig. 1b). Arrows show the direction of the applied magnetic field variation.

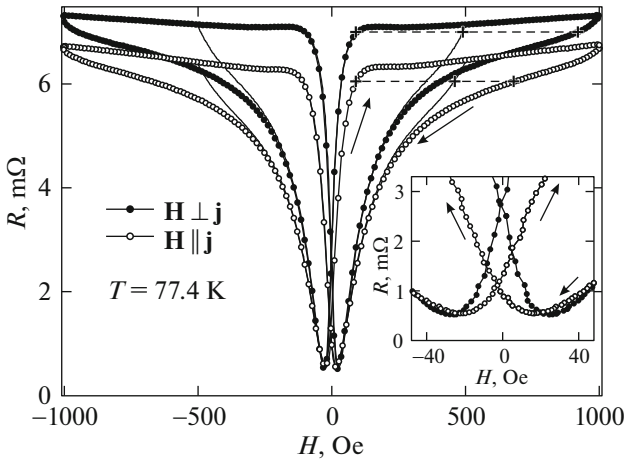

Fig. 3. Hysteretic field dependences of magnetoresistance $R(H)$ for the investigated sample at maximum applied fields of H_{app} = 500 and 1000 Oe for the indicated configurations (schematic of the experiment is shown in Fig. 1b). Arrows show the direction of the applied field variation. Solid lines show the reverse $R(H_\downarrow)$ dependences at H_{app} = 500 Oe. Horizontal lines illustrate determination of the hysteresis field width ΔH at $H_\uparrow$ = 90 Oe. Inset: $R(H)$ dependences in weak fields.

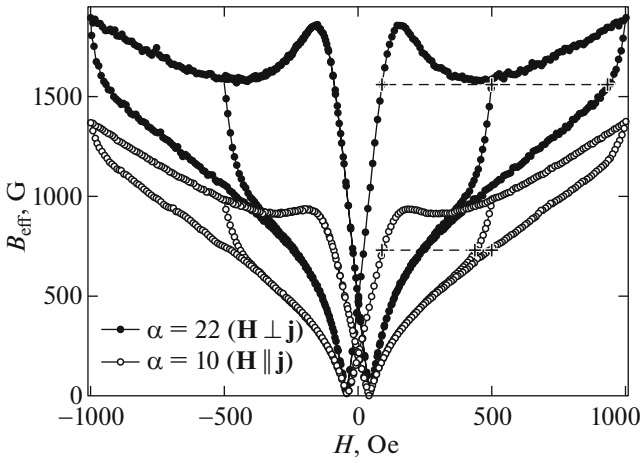

Fig. 4. Hysteretic field dependences of the effective field $B_{eff}(H)$ in the intergrain medium (absolute value of Eqs. (3) and (4)) obtained using the $M(H)$ data from Fig. 2 at two α values for the perpendicular and parallel configurations. Horizontal lines illustrate determination of the hysteresis field width ΔH at $H_\uparrow$ = 90 Oe (analogous to Fig. 3).

mentioned magnetoresistance anisotropy: $R_\perp(H) > R_\parallel(H)$. The inset in Fig. 3 shows the $R(H)$ dependences in the range of ±55 Oe. The minima in the $R(H_\downarrow)$ dependences arise under the condition of the maximum compensation of the field $\mathbf{B}_{ind}$ induced by the grain magnetic moments by the applied field. At the $H_\downarrow$ values smaller than ~50 Oe, the $M(H_\downarrow)$ value is positive (Fig. 2) and the terms in the right-hand side of Eq. (4) have different signs, which leads to the occurrence of the minimum in the $B_{eff}(H_\downarrow)$ and $R(H_\downarrow)$ dependences.

The horizontal lines in Fig. 3 show an example of determination of the magnetoresistance hysteresis width $\Delta H = |H_\uparrow - H_\downarrow|$ at the same value $H_\uparrow$ = 90 Oe. It can be seen that the ΔH value (the difference between the fields $H_\uparrow$ and $H_\downarrow$ at which the horizontal straight crosses the $R(H_\downarrow)$ dependences) for $R_\perp(H)$ is noticeably higher than the ΔH value for the $R_\parallel(H)$ dependence. As was established previously [22–24], the parameter ΔH at one chosen orientation of **H** and **j** is independent of the transport current in a wide range of this quantity.

To determine the α values at the parallel and perpendicular orientations, we used the magnetic measurement data (Fig. 2) and built the hysteretic $B_{eff}(H)$ dependences using Eqs. (3) and (4). Since the magnetoresistance is determined by the absolute value of B_{eff} rather than by its direction ($R \propto |B_{eff}|$), we took the absolute value of the $B_{eff}(H)$ function. Then, the α values were chosen so that the value $\Delta H = H_\downarrow - H_\uparrow$ determined directly from the $B_{eff}(H_\uparrow)$ and $B_{eff}(H_\downarrow)$ dependences was similar to the $\Delta \boldsymbol{H}$ value obtained from the experimental $R(H)$ dependences (Fig. 3). In this case, the $R_\perp(H)$ and $R_\parallel(H)$ dependences were compared using the $M_\perp(H)$ and $M_\parallel(H)$ data. In addition, we made one more assumption: in Eqs. (3) and (4), the difference between projections of the vector **H** for the **H** ∥ **j** and **H** ⊥ **j** orientations was ignored.[1]

The best agreement in the wide field range (see below) was observed at α ~ (22–25) for the perpendicular configuration and α ~ (10–15) for the parallel configuration. The larger α values describe better the data for the field range of 500–100 Oe, which is apparently due to the fact that the condition $\alpha \neq f(H)$ is only met in the first approximation (see Section 2).

Figure 4 shows the obtained $B_{eff}(H)$ dependences for α = 10 and 22. The horizontal lines illustrate the determination of the ΔH value at $H_\uparrow$ = 90 Oe for these configurations, similarly to the example for the $R(H)$ dependences in Fig. 3. It can be seen that a decrease in ΔH for the parallel configuration related to the smaller parameter α is reproduced well at this approach.

Figure 5 shows the data on the dependences of ΔH on $H_\downarrow$ (the lengths of the horizontal portions between $H_\downarrow$ and $H_\uparrow$ in Figs. 3 and 4 at R = const and B_{eff} = const) obtained in the maximum applied field of

[1] Obviously, for a polycrystal the angle θ in the expression for the projection of **H** onto the **j** direction ($H\sin\theta$) will not be strictly 0 and 90° at the **H** for the **H** ∥ **j** and **H** ⊥ **j** orientations. In these cases, the variation in the effective angle θ leads to the occurrence of additional fitting parameters, although, according to our estimations, does not drastically affect our conclusions concerning the larger α value at the perpendicular configuration.

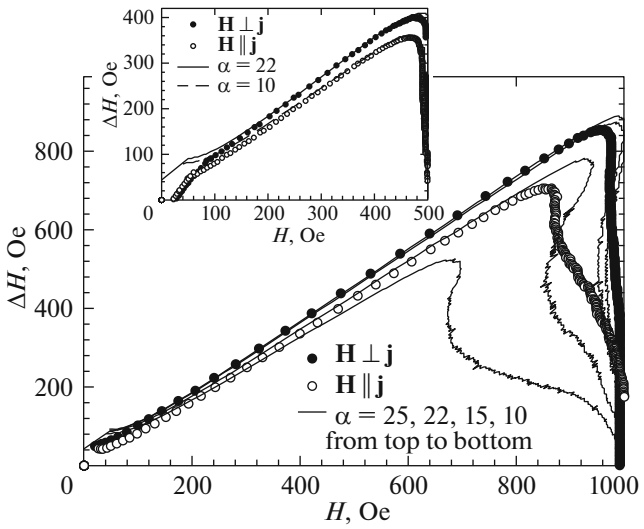

Fig. 5. Dependences of the hysteresis field width ΔH on $H_{\downarrow}$ obtained from the $R(H)$ dependences (dots) and from the $B_{\text{eff}}(H)$ dependences using Eqs. (3) and (4) (lines) at different α values. The data for $H_{\text{app}} = 1000$ Oe are shown. Inset: the data for $H_{\text{app}} = 500$ Oe.

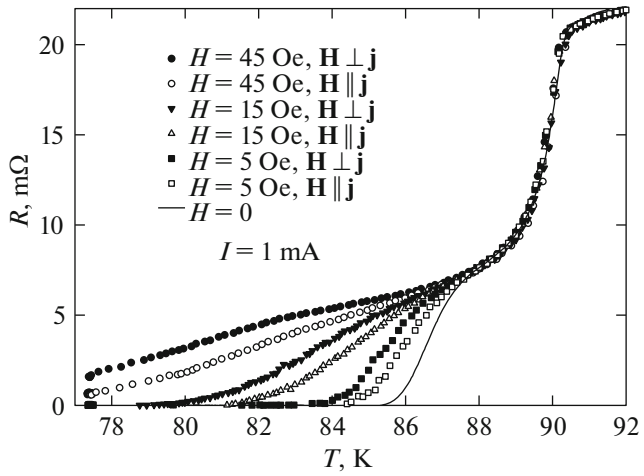

Fig. 6. ZFC $R(T)$ dependences in different applied fields at different mutual orientations of **H** and **j** in the resistive transition region.

$H_{\text{app}} = 1000$ Oe from the hysteretic $R(H)$ dependences (dots) and $B_{\text{eff}}(H)$ dependences (lines). The calculated $\Delta H(H_{\downarrow})$ dependences were obtained at several α values. The inset in Fig. 5 shows the data obtained at $H_{\text{app}} = 500$ Oe. Despite the certain spread of the α values in fields of up to 500 Oe and 500–1000 Oe, good agreement between the experimental and calculated $\Delta H(H_{\downarrow})$ dependences allows us to state that at the parallel configuration $\mathbf{H} \parallel \mathbf{j}$, the parameter α is almost twice as small as its value at $\mathbf{H} \perp \mathbf{j}$. This confirms our assumptions (see Section 2) on the character of magnetic induction line crowding in the intergrain medium.

4.2. Anisotropy of the R(T) Dependences

The above statement is confirmed also by the effect of the mutual orientation of **H** and **j** on the resistive transition. Figure 6 shows the $R(T)$ dependences for the investigated sample in the region of the resistive transition at $\mathbf{H} \parallel \mathbf{j}$ and $\mathbf{H} \perp \mathbf{j}$. The sharp resistance growth corresponds to the transition in HTS grains and the smooth portion of the $R(T)$ dependences, to the transition in the intergrain boundary subsystem [17, 24–26]. It can be seen that the difference between the $R(T)$ dependences for $\mathbf{H} \parallel \mathbf{j}$ and $\mathbf{H} \perp \mathbf{j}$ is observed earlier in the temperature range corresponding to the resistive transition in the intergrain medium [7, 10].

Let us use the aforementioned approach to estimate the temperature evolution of the effective field in the intergrain medium. The ZFC $M(T)$ dependences, analogously to the $R(T)$ dependences in Fig. 6, are shown in Fig. 7 in the bottom. Figure 8 presents temperature dependences of the effective field in the intergrain medium obtained from Eq. (3) with regard to the $M(T)$ data: $B_{\text{eff}}(T) = -4\pi M(T)\alpha + H$. In the calculation of these dependences, the α values were the same as in building the $B_{\text{eff}}(H)$ dependences shown in Fig. 4, i.e., $\alpha = 10$ at $\mathbf{H} \parallel \mathbf{j} \parallel \mathbf{L}$ and $\alpha = 22$ at $\mathbf{H} \perp \mathbf{j}$. In this case, it can be seen that the main difference between the behaviors of the resistive transition is due to the different effective fields in the intergrain medium, which changes monotonically with increasing external field and, additionally, with the change of the parallel orientation for the perpendicular one.

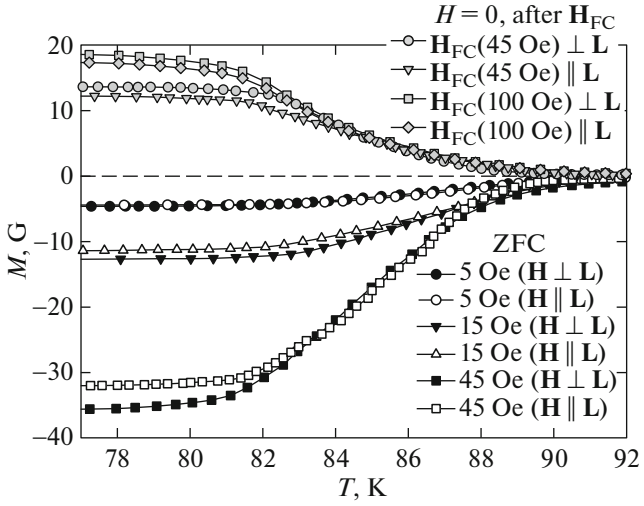

Fig. 7. In the bottom (negative M values): ZFC temperature dependences of the magnetic moment $M(T)$ for the investigated sample in different external fields and different mutual orientations of **H** and **L** (see Fig. 1b). On the top (positive M values): FC $M(T)$ dependences obtained with subsequent switching off of the applied field ($H = 0$).

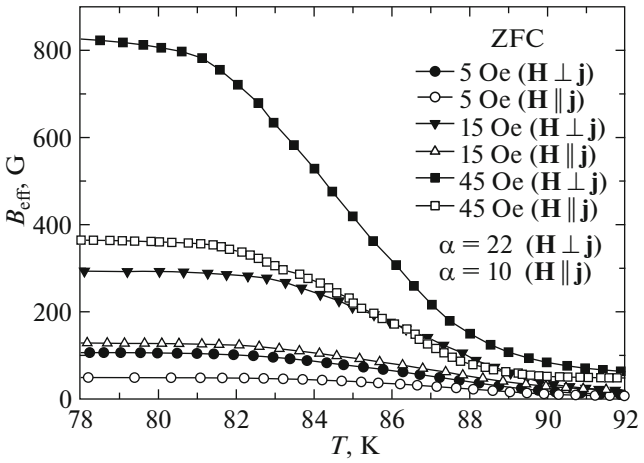

Fig. 8. ZFC temperature dependences of the effective field in the intergrain medium at different mutual orientations of **H** and **j** obtained for two α values from the $M(T)$ data from Fig. 7.

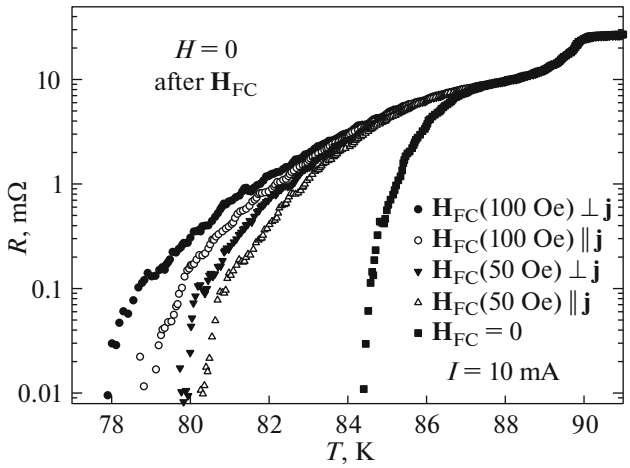

Fig. 9. $R(T)$ dependences for the investigated sample in zero applied field near the resistive transition. Cooling was performed in an applied field at different mutual orientations of **H** and **j**; after that, the applied field was switched off.

As is known, after the FC procedure, the sample has the negative magnetic moment, but with the smaller absolute value as compared with the case of the ZFC conditions. Then, after switching off the field, the magnetic moment of the sample takes the positive value due to the trapped flux. The $M(T)$ dependences measured in zero external field (after the FC procedure) are shown in Fig. 7 (on the top). After this thermomagnetic prehistory, the distribution of the induced fields in the intergrain medium will be analogous to that shown in Fig. 1b for the case of cooling at $\mathbf{H}_{FC} \perp \mathbf{j}$ and Fig. 1c for $\mathbf{H}_{FC} \parallel \mathbf{j}$, but here there is no external field ($\mathbf{H} = 0$) and the directions of $\mathbf{B}_{ind}$ and $\mathbf{M}_G$ vectors changed for the opposite ones, which, however, do not matter for the current flow.

In the investigated case, similar to the ZFC $R(H)$ and $R(T)$ dependences, the $R(T)$ dependences for $\mathbf{H}_{FC} \perp \mathbf{j}$ and $\mathbf{H}_{FC} \parallel \mathbf{j}$ will be different. This behavior is illustrated in Fig. 9. All the data in Fig. 9 were obtained in zero applied field, although the thermomagnetic prehistories were different. The analogous behavior of the $R(T)$ dependences is observed after the ZFC procedure with the subsequent switching on/off the applied field $\mathbf{H}_{app} = 500$ Oe (not shown).

It should be noted that the difference between the $R(T)$ dependences at $\mathbf{H}_{FC} \perp \mathbf{j}$ and $\mathbf{H}_{FC} \parallel \mathbf{j}$ is not as much (Fig. 9) as at $\mathbf{H}_{ZFC} \perp \mathbf{j}$ and $\mathbf{H}_{ZFC} \parallel \mathbf{j}$ (Fig. 6) and is pronounced only in the logarithmic scale by R. This is apparently due to the invalidity of the condition $\alpha =$ const (see Section 2) in such a wide field range. Indeed, there is the discrepancy between the experimental and calculated $\Delta H(H_\downarrow)$ dependences (Fig. 5) in fields $H_\downarrow$ below ~100 Oe. The minima in the experimental $R(H_\downarrow)$ dependences (inset in Fig. 3) are observed at $H_\downarrow \sim 25$ and ~18 Oe for $\mathbf{H} \perp \mathbf{j}$ and $\mathbf{H} \parallel \mathbf{j}$, respectively. At $\alpha = 22$ ($\mathbf{H} \perp \mathbf{j}$) and 10 ($\mathbf{H} \parallel \mathbf{j}$), the $B_{eff}(H_\downarrow)$ dependences (Fig. 4) have the minima at the higher $H_\downarrow$ values (~45 and 40 Oe). To adjust the $B_{eff}(H_\downarrow)$ minima with the $R(H_\downarrow)$ minima within the approach used, it is necessary to use smaller α values (~2.2 and ~1.5) for the orientations $\mathbf{H} \perp \mathbf{j}$ and $\mathbf{H} \parallel \mathbf{j}$, respectively. The conditions of the thermomagnetic prehistory for the regime $H \to +H_{app} \to H = 0$ (similarly to the $R(H)$ dependences) and the FC mode with the subsequent switching off of the field (Fig. 9) are analogous and, according to the critical state model, the trapped flux remains mainly at the grain center. It is natural that in these cases the effect of the trapped flux on the intergrain medium will be weaker than when the screening currents flow mainly near the grain surface (with increasing external field $H = H_\uparrow$ after the ZFC procedure). This explains the weaker flux compression in weak fields (at $H = H_\downarrow$) and smaller α values. Nevertheless, the difference between the cases of $\mathbf{H}_{FC} \perp \mathbf{j}$ and $\mathbf{H}_{FC} \parallel \mathbf{j}$ is observed even in zero applied field (Fig. 9) and is related to the effect of the flux trapped in grains on the intergrain medium.

5. CONCLUSIONS

Thus, it was demonstrated that the observed anisotropy (magnetic field–transport current) of the magnetoresistive properties of granular HTSs is caused by the magnetic flux compression in the intergrain medium. At different mutual orientations of **H** and **j**, the transport current chooses mainly the trajectories at which intergrain tunneling occurs along the direction corresponding to the smallest angle between $\mathbf{B}_{ind}$ and **j**, where the magnetic induction lines are the most rarified. At the parallel configuration ($\mathbf{H} \parallel \mathbf{j}$), the

effective degree of magnetic flux compression is approximately twice as lower than at the perpendicular configuration ($\mathbf{H} \perp \mathbf{j}$). This is valid in a fairly wide field range (from ~10^2 to 10^3 Oe). As the external field further increases or the temperature approaches T_C, the effect of the grain magnetic moments on the intergrain medium weakens and the second term in Eq. (2) becomes larger than the first term. In this case, the observed magnetoresistance anisotropy decreases, i.e., the value $R(\mathbf{H} \parallel \mathbf{j})/R(\mathbf{H} \perp \mathbf{j})$ approaches unity, in accordance with the model representations proposed in [7].

ACKNOWLEDGMENTS

The authors thank M.I. Petrov and K.Yu. Terent'ev for sample preparation, A. Krasikov and A.L. Freidman for help, and A.A. Dubrovskii for discussions.

This study was supported by the Russian Foundation for Basic Research, Government of the Krasnoyarsk Territory, and Krasnoyarsk Territorial Foundation for Support of Scientific and R&D Activities, project no. 16-48-243018.

REFERENCES

1. D. Lopez and F. de la Cruz, Phys. Rev. B **43**, 11478 (1991).
2. D. Lopez and R. Decca, and F. de la Cruz, Solid State Commun. **79**, 959 (1991).
3. D. Lopez and R. Decca, and F. de la Cruz, Supercond. Sci. Technol. **5**, 276 (1992).
4. M. M. Asim and S. K. Hasanin, Solid State Commun. **80**, 719 (1991).
5. A. Kilic, K. Kilic, S. Senoussi, and K. Demir, Physica C **294**, 203 (1998).
6. O. V. Gerashchenko and S. L. Ginzburg, Supercond. Sci. Technol. **13**, 332 (2000).
7. D. Daghero, P. Mazzetti, A. Stepanescu, and P. Tura, Phys. Rev. B **66**, 11478 (2002).
8. A. A. Sukhanov and V. I. Omelchenko, J. Low Temp. Phys. **29**, 297 (2003).
9. D. A. Balaev, A. G. Prus, K. A. Shaikhutdinov, and M. I. Petrov, Tech. Phys. Lett. **32**, 677 (2006).
10. D. A. Balaev, A. G. Prus, K. A. Shaukhutdinov, D. M. Gokhfeld, and M. I. Petrov, Supercond. Sci. Technol. **20**, 495 (2007).
11. V. V. Derevyanko, T. V. Sukhareva, and V. A. Finkel', Phys. Solid State **46**, 1798 (2004).
12. V. V. Derevyanko, T. V. Sukhareva, and V. A. Finkel', Phys. Solid State **49**, 1829 (2007).
13. T. V. Sukhareva and V. A. Finkel', Phys. Solid State **50**, 1001 (2008).
14. J. Bardeen and M. J. Stephen, Phys. Rev. **140**, A1197 (1965).
15. W. K. Kwok, U. Welp, G. W. Crabtree, K. G. Vandervoot, R. Hulscher, and J. Z. Liu, Phys. Rev. Lett. **64**, 966 (1990).
16. D. A. Balaev, S. I. Popkov, E. I. Sabitova, S. V. Semenov, K. A. Shaykhutdinov, A. V. Shabanov, and M. I. Petrov, J. Appl. Phys. **110**, 093918 (2011).
17. D. A. Balaev, S. V. Semenov, and M. I. Petrov, Phys. Solid State **55**, 2422 (2013).
18. D. A. Balaev, S. V. Semenov, and M. I. Petrov, J. Supercond. Novel. Magn. **27**, 1425 (2014).
19. D. A. Balaev, S. I. Popkov, K. A. Shaikhutdinov, M. I. Petrov, and D. M. Gokhfeld, Phys. Solid State **56**, 1542 (2014).
20. D. A. Velikanov, RF Patent No. 2339965, Byull. Izobret. No. 33 (2008).
21. D. M. Gokhfeld, Phys. Solid State **56**, 2380 (2014).
22. D. A. Balaev, D. M. Gokhfeld, A. A. Dubrovski, S. I. Popkov, K. A. Shaikhutdinov, and M. I. Petrov, J. Exp. Theor. Phys. **105**, 1174 (2007).
23. D. A. Balaev, A. A. Dubrovskii, K. A. Shaikhutdinov, S. I. Popkov, D. M. Gokhfeld, Yu. S. Gokhfeld, and M. I. Petrov, J. Exp. Theor. Phys. **108**, 241 (2009).
24. D. A. Balaev, A. A. Dubrovskii, S. I. Popkov, D. M. Gokhfeld, S. V. Semenov, K. A. Shaykhutdinov, and M. I. Petrov, Phys. Solid State **54**, 2155 (2012).
25. V. V. Derevyanko, T. V. Sukhareva, V. A. Finkel', and Yu. N. Shakhov, Phys. Solid State **56**, 649 (2014).
26. D. A. Balaev, A. A. Bykov, S. V. Semenov, S. I. Popkov, A. A. Dubrovskii, K. A. Shaikhutdinov, and M. I. Petrov, Phys. Solid State **53**, 922 (2011).

Translated by E. Bondareva